Open Access

Journal of Energy and Power Technology

LIDSEN Publishing Inc.

Short Communication

Electrochemical Impedance Spectroscopic Studies of PHEV2 form-factor Lithium-ion Cells for Automotive Applications

Simon Calles [1], Paul Heitjans [2], Alexander Börger [3, *]

1. LetterBox 1581, Volkswagen AG, Berliner Ring 2, D-38436 Wolfsburg, Germany; E-Mail: simon.calles2@volkswagen.de
2. Institute of Physical and Electrochemistry, Leibniz University Hanover, Callinstr. 3a, D-30167 Hannover, Germany; E-Mail: heitjans@pci.uni-hannover.de
3. LetterBox 1723, Volkswagen AG, Berliner Ring 2, D-38436 Wolfsburg, Germany; E-Mail: alexander.boerger@volkswagen.de

* **Correspondence:** Alexander Börger; E-Mail: alexander.boerger@volkswagen.de

Academic Editor: Ahamed Irshad

Special Issue: Batteries: Past, Present and Future

Journal of Energy and Power Technology
2022, volume 4, issue 2
doi:10.21926/jept.2202015

Received: November 09, 2021
Accepted: April 10, 2022
Published: April 18, 2022

Abstract

Prismatic PHEV2 form-factor lithium-ion cells with a nominal capacity of 25 Ah (as used for automotive applications) have been studied with electrochemical impedance spectroscopy (EIS). The data was evaluated using electrical equivalent circuits. Mathematical modeling, system identification, and the determination of model parameters of the lithium-ion cell were also carried out. While a study of the influence of temperature and state-of-charge (SOC) performed using pristine lithium-ion cells showed a nonlinear relationship between temperature and the fits for different RC elements. Finally, the interdependency of parameters determined by EIS has been demonstrated for cells in different aging regimes (cyclic vs. non-cyclic aging) relevant for automotive requirements use cases.

Keywords

Impedance spectroscopy; lithium-ion batteries; PHEV2 format; automotive applications

1. Introduction

Lithium-ion batteries are one of the key technologies for solving the energy storage problems associated with portable and automotive applications [1, 2]. Performance characteristics such as an extended cycle behavior and long life are of critical importance for these batteries [3, 4]. However, aging mechanisms that lead to battery degradation [5-10] reduce both the range and period of the possible use of electric cars. Thus, good battery management systems (BMS) are needed to improve the performance and aging characteristics of lithium-ion batteries.

Electrochemical impedance spectroscopy (EIS) is a valuable tool for studying electrochemical systems such as batteries [11-15]. EIS offers a means of improving the performance and functionality of BMS by providing precise charge and capacity determinations. However, several obstacles have to be overcome before laboratory EIS measurements can be transferred to a BMS working in a real car-. One such obstacle is that the time - impedance measurements in the laboratory are often too long - several hours - for the rapidly changing battery characteristic encountered in a real car. One possible solution to this is faster measurements based on, for example, multisine methods [16, 17].

A realization of EIS in real traction batteries requires several basic investigations of the properties of the cells to guarantee that the measurements results are reliable and reproducible. The investigations presented in the current study have been done in this vein and continue the work begun by other researchers on direct EIS excitation signals [18-25]. While alternative approaches exist, such as passive approaches that capture signals already generated within the car [26], the direct approach taken here offers several advantages, such as requiring less real-time computer power.

2. Experimental

2.1 Instrumentation

The majority of the impedance measurements were done with a Digatron EIS-Meter outputting 2 A across a frequency band of 5 kHz-10 mHz. Multisine measurements were done with a Biologic VMP3, and the measurements for the variation of the excitation current amplitude were done with a Gamry Reference 3000 Potentiostat and 30 k booster. The multisine measurements were used only for frequencies below 1 Hz and with a reduced excitation amplitude (0.3 mV) for a maximum of 20 single frequencies and 2 decades.

2.2 Test Cells

The cells used in this study were prismatic lithium-ion cells manufactured by Panasonic with a nominal capacity of 25 Ah in a PHEV 2 (PHEV = plug-in hybrid electric vehicle) form factor. The cells contain $Li(Ni_{0.33}Mn_{0.33}Co_{0.33})O_2$ as the cathode material and graphite as the anode material. In general, each experiment was done with at least three different cells.

2.3 Electrochemical Investigations

2.3.1 Influence of Spatial Configuration

In a real traction battery, cells can be built in different spatial configurations depending on the available space - principally, either standing, lying flat, or upright (see Figure 1). To prove that these different orientations do not influence the sensitivity of the EIS measurements, measurements were done in all three orientations and then compared. For these measurements, the cell was first pre-conditioned with five 1 *C* full cycles between the voltage borders, including a constant current/constant voltage (CCCV) recharge until I < C_n/20. After a stable electr(ochem)ical state had been reached in this way (equilibration time at least 1 h), the cell was allowed to reach an operating point of 65% of the state of charge (SOC), and then the impedance characteristics of the cell were measured. The cell was then tested in a different orientation before being tested a second time in the original orientation to confirm that no significant changes in the cell have occurred.

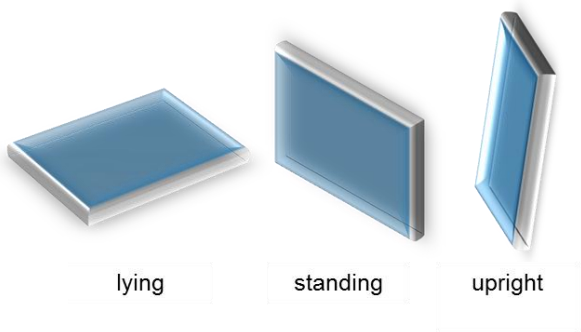

Figure 1 Principal special configurations of cells in vehicles.

2.3.2 Influence of Signal Form and Strength (Excitation Current Amplitude)

Pre-conditioning with five 1 *C* full cycles as in 2.3.1, above, was carried out until the cell reached an operating point of around 50% SOC. The impedance spectra were then measured with different current amplitudes to determine the border current and border frequencies between which there is a linear system response to the initial excitation.

It has been reported that multisine excitation shortens measurements times in impedance spectroscopy [16, 17]. In this study, impedance spectra were captured at the operating point using different excitation modes both to study the role that multisine excitation plays in the reduction of measurement time and to analyze signal quality.

2.3.3 Influence of Temperature

Figure 2 shows the measurement setup that was used to investigate the influence of temperature on the sensitivity of impedance spectroscopy. Pre-conditioning, as in 2.3.1, above was carried out until the cell reached an operating point of about 50% SOC. It was then placed inside the temperature chamber and left for 3 h to reach a homogeneous temperature distribution before measurements began. Each measurement was repeated with a 10 min interval between repetitions

to ensure the reliability and reproducibility of the measurements. Measurements were taken at several temperatures, with a thermal equilibration period of at least 1 h at each temperature.

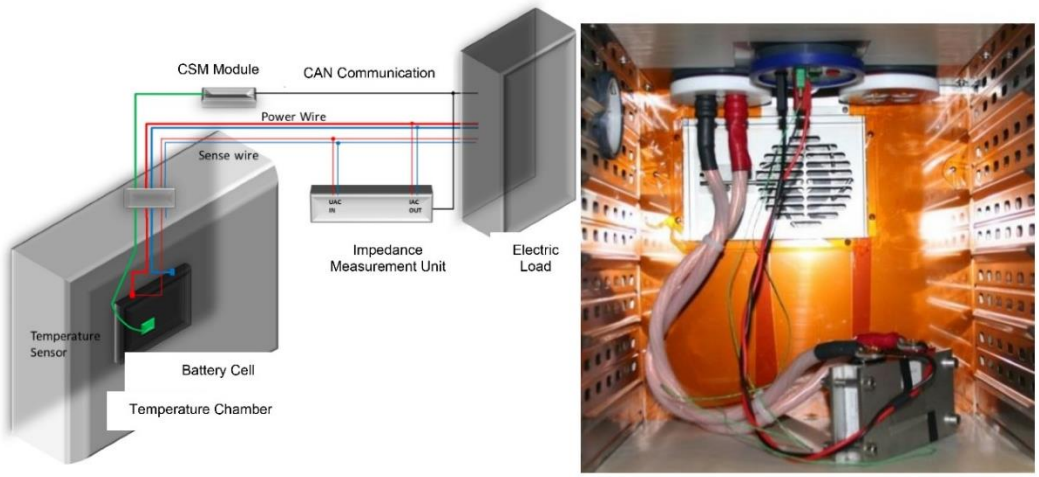

Figure 2 Measurement setup for studying the influence of temperature on EIS measurements.

2.3.4 Influence of Pressure

The aging of lithium-ion cells gives rise to an increase in thickness of the solid-electrolyte interface (SEI) that cause the cell to expand. The influence of these expansion forces on the impedance characteristics can be modeled using a cell that is compressed externally by a compression device, as shown in Figure 3.

Figure 3 Measurement setup for studying the influence of pressure on EIS measurements.

Pre-conditioning, as in 2.3.1, above was carried out until the cell reached an operating point of about 65% SOC. Then impedance measurements were made while the cell was subjected to a range of external forces. The experiments were done with different compression plates to guarantee that the cell housing does not absorb all the force. The operating point of the cell remains constant during these measurements.

2.3.5 Influence of the State-of-Charge

After pre-conditioning, as in 2.3.1, above, cells were allowed to reach a range of different operating points (100, 80, 65, 50, 35, and 20% SOC). After each operating point was reached, the cell was left for 30 min, and then its impedance spectrum was recorded. After another 10 min break, a further measurement was done. This procedure was done with both a pristine cell and an aged cell with a state-of-health (SOH) of 80%.

2.3.6 Parameter Precision

The degree of precision for the different parameters were: +/-2 K (temperature), +/-0.5% SoC, and +/-5% in frequency.

3. Results and Discussion

3.1 Influence of Spatial Configuration

As Figure 4 shows, the orientation of the cell had no significant impact, besides tiny differences in the diffusive branches, on the impedance spectra of the cell. And the subtle differences in the diffusive branches are probably due to reaching the borders of the applicability of the method rather than orientation effects. For automotive applications, this is a positive result because it allows individual cells in the complete battery pack to be orientated differently. However, orientation could influence the thermal properties of a real battery pack, so this finding should be reinvestigated when EIS is used for the characterization of complete battery packs, rather than single cells, as in this current study.

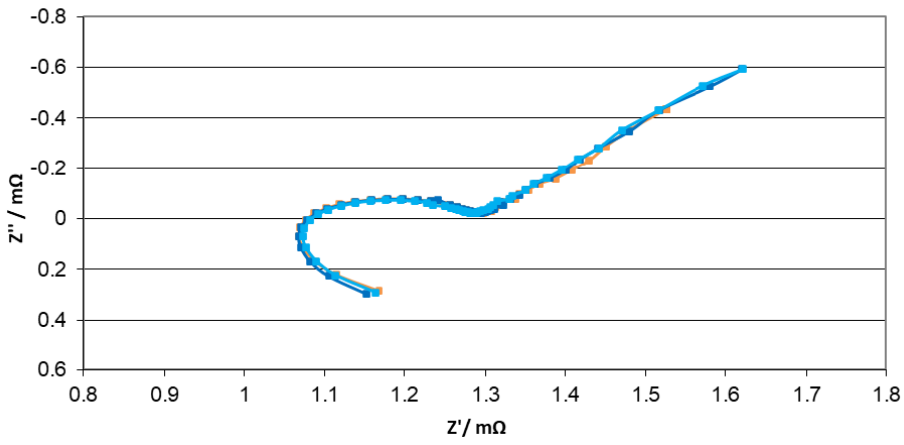

Figure 4 Impedance measurements with various cell orientations. Orange: lying flat, light blue: standing, dark blue: upright (see Figure 1 for definitions).

3.2 Influence of Signal Form and Strength

3.2.1 Influence of Signal Strength

The influence of signal strength on EIS measurements is shown in Figure 5a (Nyquist plot) and Figure 5b (Bode plot). The results show that there is a linear system response up to a border current of 10 A and down to a border frequency of 1 Hz. At a border current of 20 A (note: measurements with higher current were not possible), the border frequency reduces to 315 Hz. At lower frequencies, the system displayed a nonlinear response, as shown by the change of the phase angle in the Bode plot, since the spectra do not coincide with the ones with lower excitation currents. This interpretation is supported by the fact that the experimental setup (wiring, shielding, etc.) has much more of an influence at high frequencies than at low frequencies. Although this interpretation could not be confirmed - by analyzing the harmonic distortion of the voltage response, for example, or Kramers-Kronig relations - due to the limited number of measurements, it was held to be valid.

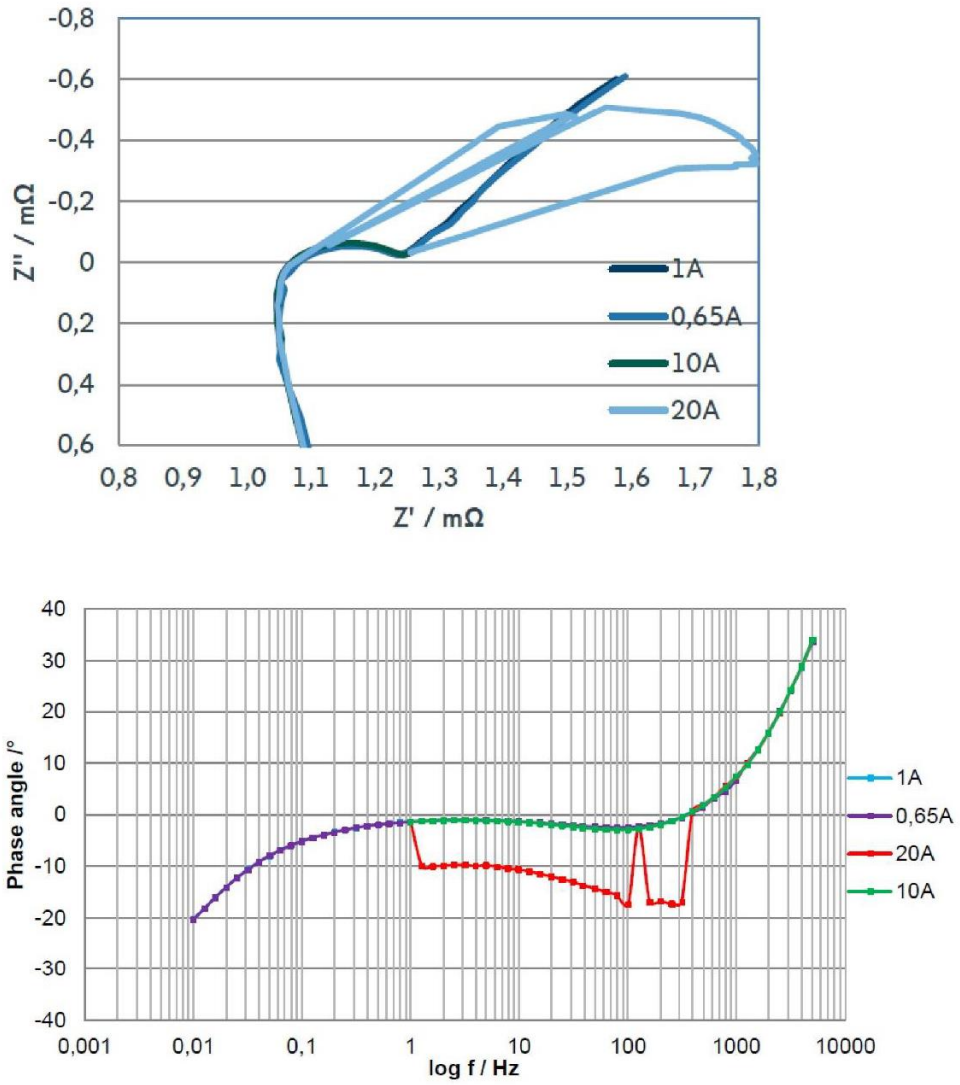

Figure 5 Impedance measurements under variation of signal strength. (a, top) Nyquist plot, (b, bottom) Bode plot. The blue curve corresponds to the multisine measurement, and the red curve corresponds to the conventional single sine measurement.

3.2.2 Influence of Signal Form

To compare the quality of impedance data when multisine excitation is used as in references [16] and [17], impedance data were taken in normal and in multisine mode at the same operating point. In single frequency excitation mode, the best results were obtained with an excitation amplitude of 3 mV, as shown in Figure 6. Due to equipment limitations, the excitation amplitude for the multisine measurement had to be limited to 1 mV, and real multisine measurements could be done only for frequencies up to 1 Hz. The results for the multisine measurements are shown in the Bode and Nyquist plots presented in Figure 6a and Figure 6b, respectively.

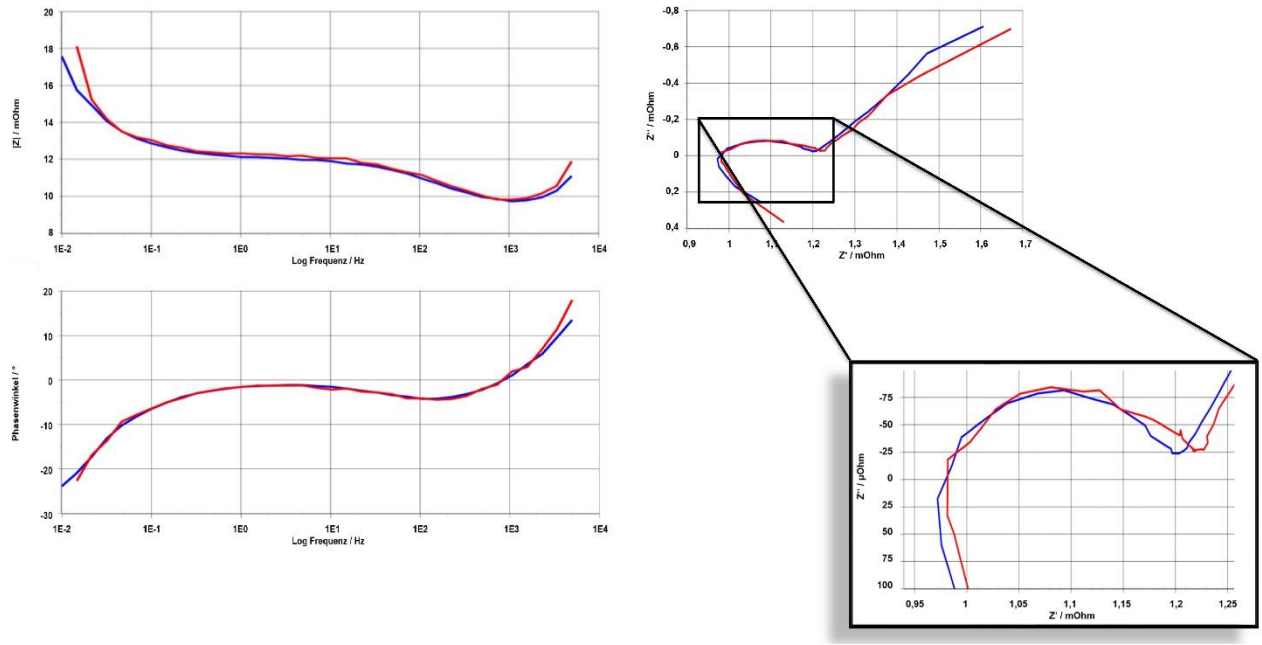

Figure 6 The influence of signal form on the impedance measurements: (a, left) Bode plots. (b, top right): complete spectrum in Nyquist plot, (b, bottom right): extension of Nyquist plot. The blue curve is the multisine measurement, and the red curve is the conventional single sine measurement.

The Nyquist diagram in Figure 6b shows small deviations in the middle of the frequency region that can be explained by the variation in the excitation amplitude. As the Bode plots in Figure 6a indicate that the deviations from the single-frequency measurements are less prominent in the phase angle plot, it is clear that the lower signal-to-noise ratio (SNR) of the multisine measurement is the reason for the deviation between the two measurement techniques. However, the small deviations seem acceptable because the multisine measurement takes a significantly shorter time than the conventional single-frequency technique (7 min for a complete spectrum from 5 kHz to 10 mHz -versus 21 min).

3.3 Influence of Temperature

As has already been demonstrated in studies such as [19] and [20] that describe temperature measurements with the help of impedance spectroscopy, the temperature has a significant impact on impedance measurements, particularly at some frequencies. This link is confirmed by the tests

carried out on automotive lithium-ion cells for this present study, as shown in Figure 7. The dependence is probably of the Arrhenius-type. However, the number of different temperatures used in this study is too low to differentiate between an exponential (i.e., Arrhenius-type) or polynomial dependence. Although, a pure linear dependence can be ruled out.

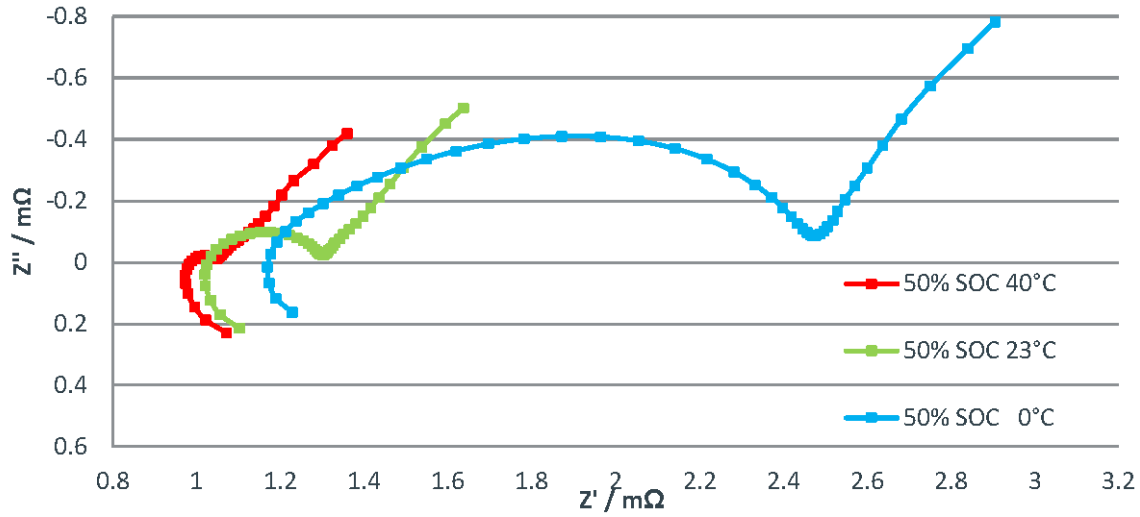

Figure 7 Influence of temperature on impedance measurements.

3.4 Influence of Pressure

As can be seen in Figure 8, the impedance spectra acquired with different external forces applied are identical. However, it remains possible that more pressure and a greater degree of mechanical deformation of the cell case could exert an influence. This would result from a forced reduction of the distance between anode and cathode, which would lead to lower resistance of the cell and an increase in the storage capacity of the double-layer. The use of different compression plates at different pressures guarantees that the external force is not fully absorbed by the cell housing. However, the external force is not high enough to cause permanent mechanical deformation of the housing. Another possible explanation for the lack of differences in the spectra is that the internal pressure inside the housing is already high enough to bring the impedance spectra to a saturation state with respect to external pressure.

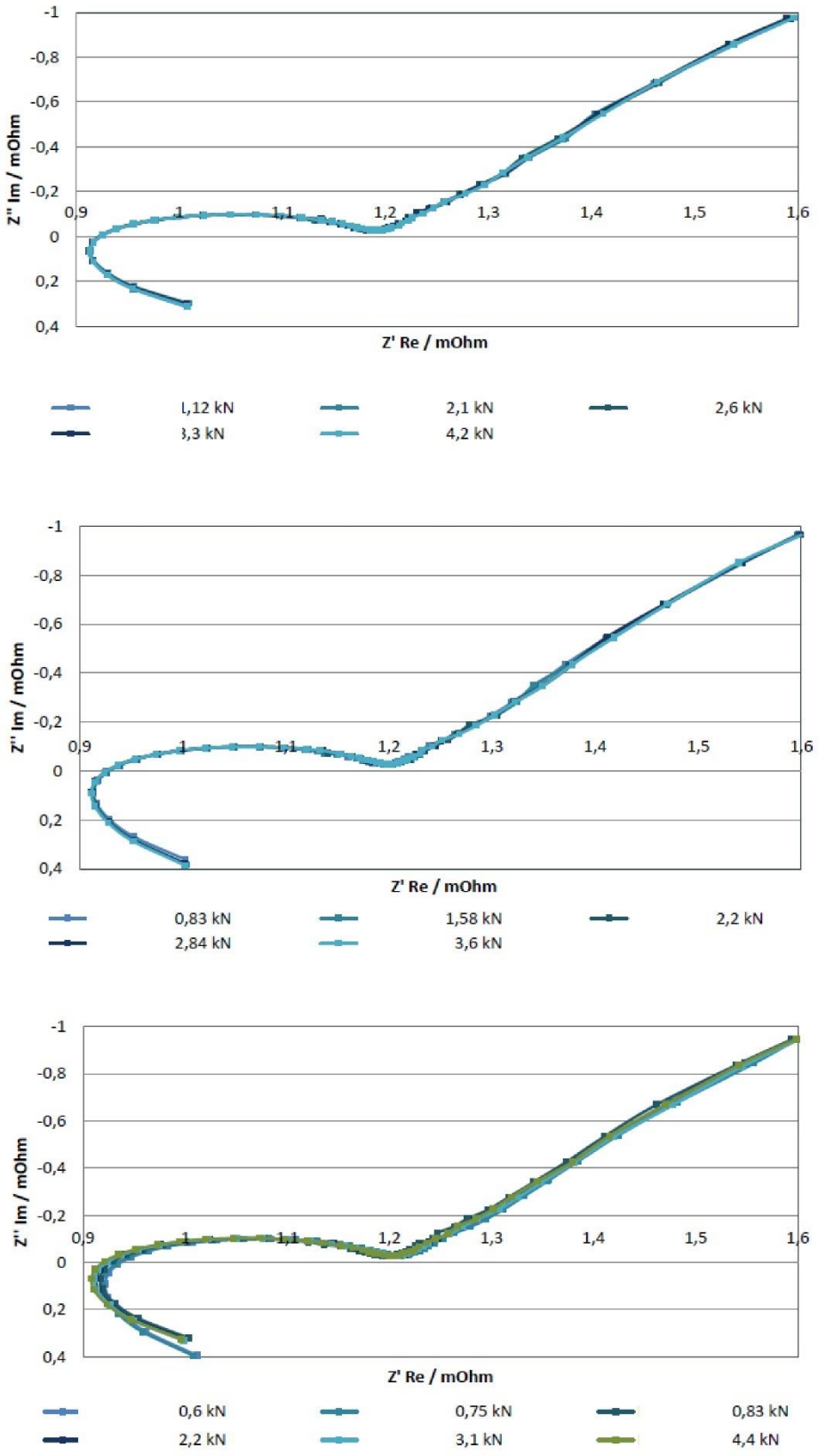

Figure 8 [Lack of] Influence of pressure on impedance measurements (experimental setup shown in Figure 3), (a, top): pressure plate cell size, (b, middle): pressure plate jelly roll size, (c, bottom): pressure plate half jelly roll size.

3.5 Influence of the State-of-Charge

Figure 9a and Figure 9b show the impedance spectra of the pristine and the aged cell, respectively, at different SOC levels. Both figures show a shift on the real axis due to an increase in Ohmic resistance and a widening and deformation of the capacitive arc. It is also clear that the differences between the spectra at different levels of SOC increase because of aging. Between 65% and 80% SOC, there is a significant difference between the spectra of the pristine and aged cells. As can be seen from Figure 10, the pristine cell shows a maximum phase angle at 65% SOC, while for the aged cell, the maximum is shifted to 80%. We also note that the maximum is prominent when the SOC level is adjusted in very small steps.

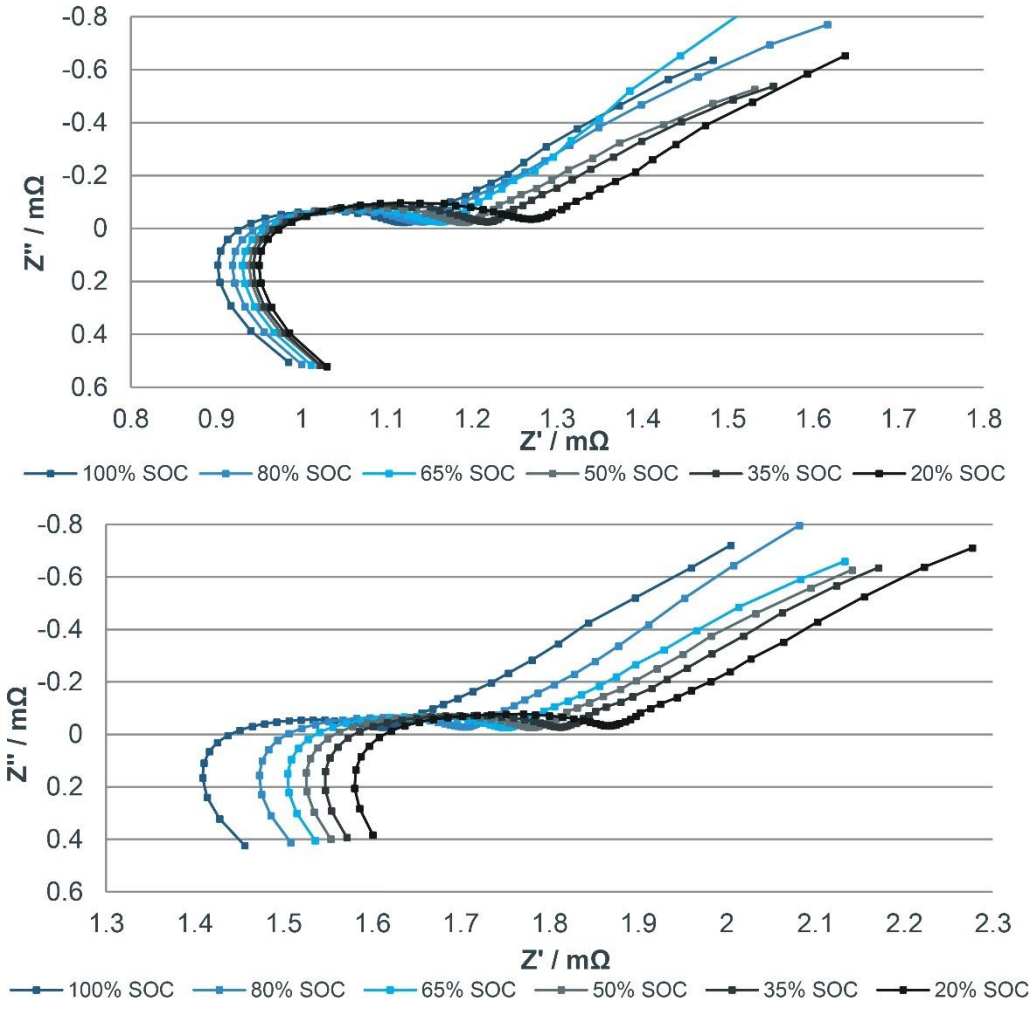

Figure 9 Influence of SOC on impedance spectra: (a, top) a pristine cell (SOH = 100%), (b, middle) an aged cell (SOH = 80%).

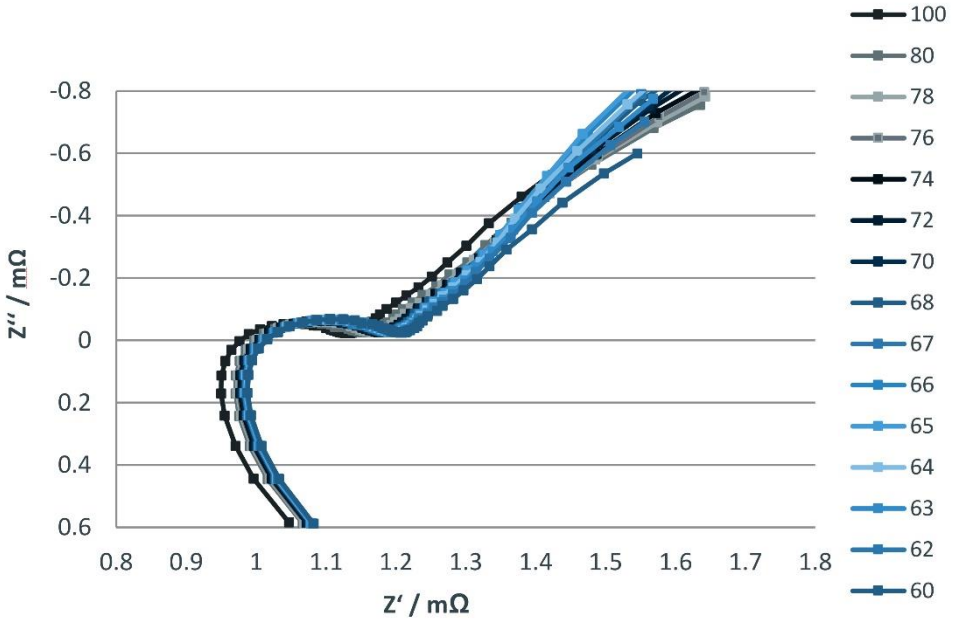

Figure 10 Variation of the phase angle in the spectrum with a maximum for SOC = 65% (pristine cell [SOH = 100%]).

This shift seems to be related to a change in the intercalation mechanism [20, 21]. Because the shift takes place at 2/3 of the anode charge, the expectation is that the shift is an anode phenomenon and correlates with the intercalation stages of graphite. This shift can also be seen in the plot of dV/dSOC versus SOC ([20] and Figure 11).

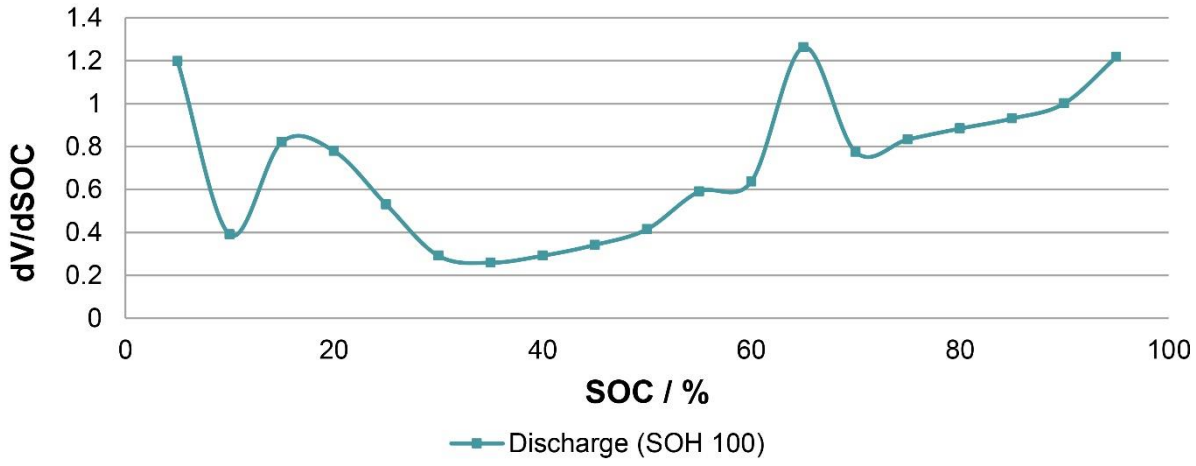

Figure 11 Plot of dV/dSOC versus SOC for a pristine cell (SOH = 100%).

A more detailed description of the changes can be made according to the evolution of the fitted elements using the equivalent circuit shown in Figure 12, which contains one pure Ohmic resistance (representing electrolyte resistance), one RL element (representing the wiring), and two RC elements (representing battery characteristics like SEI and bulk phenomena). The evolution of the resistive and capacitive elements for this equivalent circuit is shown in Figures 13a and 13b, respectively.

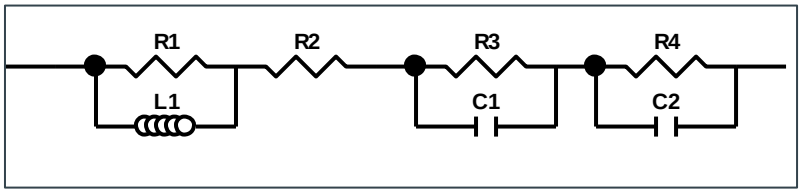

Figure 12 Electrochemical equivalent circuit used for the evaluation of impedance data of the pristine and aged cells.

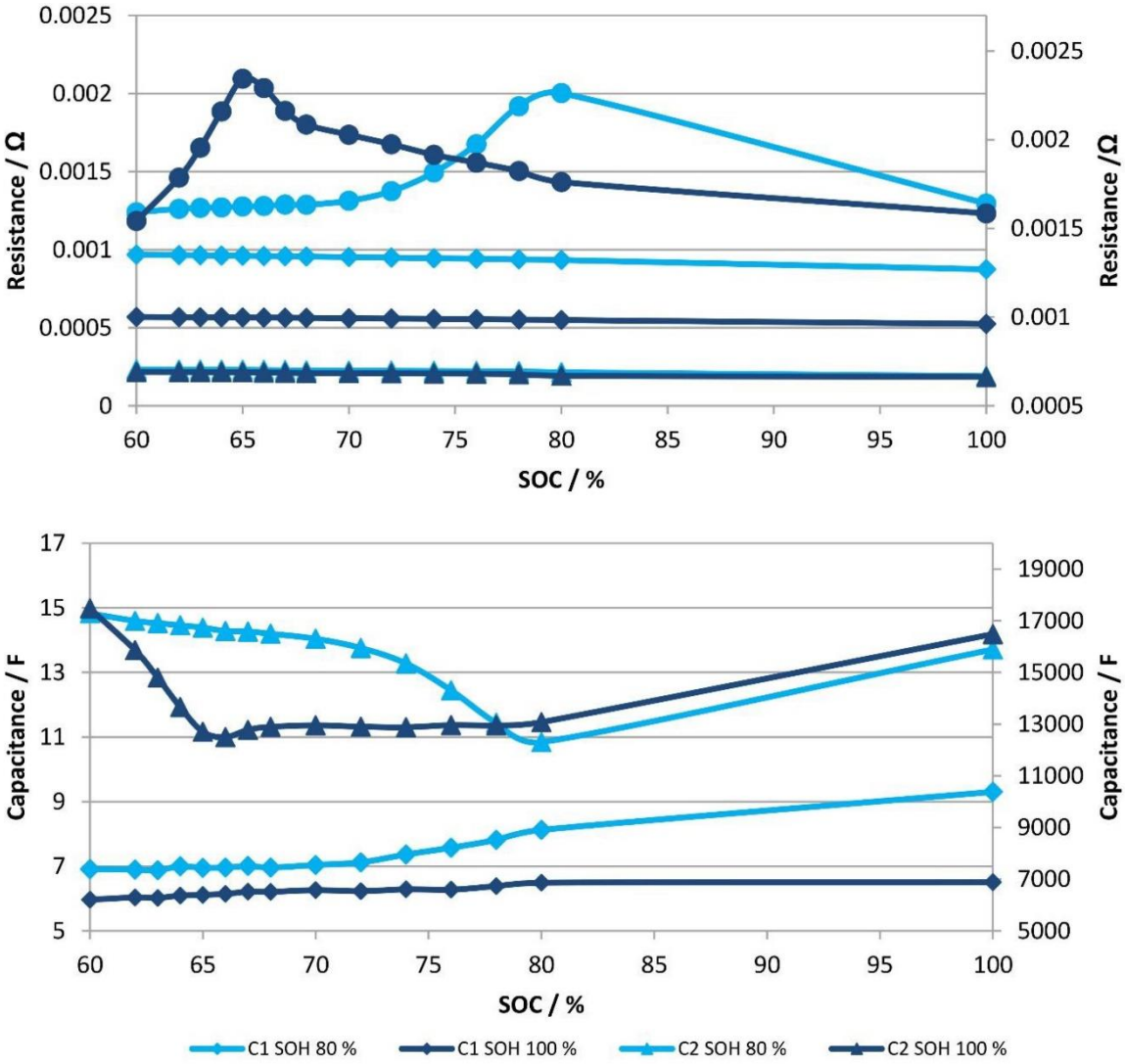

Figure 13 (a, top) Comparison of resistive elements (referring to the equivalent circuit in Figure 12) for the pristine and aged cells. Light blue curves correspond to the aged cell; dark blue curves correspond to the pristine cell; diamonds correspond to R2, triangles to R3, and circles to R4. (b, bottom) Comparison of capacitive elements (referring to the equivalent circuit in Figure 12) for the pristine and aged cells. Light blue curves correspond to the aged cell; dark blue curves correspond to the pristine cell; diamonds correspond to C1 and triangles to C2.

Figure 13a that element R2 is slightly shifted by aging, and this shift has a slight SOC dependence, while element R3, which represents the resistance to passing a phase boundary, does not show a significant aging effect. However, element R4 (the diffusion resistance) shows a remarkable shift with aging, with a maximum occurring at 65% SOC in the pristine cell shifting to 80% SOC in the aged cell. Figure 13b shows that a maximum in diffusion resistance corresponds to a minimum in the available capacity of the R||C element.

The results can be explained in terms of a change in intercalation stages from intercalation between every third to intercalation between every second graphene layer. Since the build-up or build-down of the special intercalation stage always produces stress, aging will occur faster, and more often, the intercalation boundary is passed. While conventional open-circuit voltage (OCV) curves only hint at these intercalation steps, impedance spectroscopy can detect them with great precision and a good correlation with aging characteristics. This is further proof that impedance-based battery diagnostics gives more precise data than conventional techniques, and, thus, the development of an impedance-based BMS is worthwhile.

4. Conclusions

Electrochemical impedance measurements of larger cells for automotive applications are very sensitive to temperature but (as long as the thermal environment does not change) independent of cell orientation and - within certain limits - the bracing (i.e., external pressure). The fact that such batteries retain a high sensitivity to temperature is significant for future automotive BMS development since even tiny temperature increases (resulting from, for example, micro-shorts) might be detected, suggesting that impedance spectroscopy could be used as a warning indicator for incidents like thermal-runaway propagation [27].

The comparison of impedance spectra of pristine and aged cells shows that the impedance spectra are very sensitive to specific aging phenomena, which is beneficial for better SOC and SOH monitoring. The results presented in this paper suggest that up-scaling from consumer cells to larger automotive cells does not diminish the sensitivity and thus usefulness of EIS as a diagnostic tool. In particular, the sensitivity toward the crossing of intercalation steps permits a more thorough analysis of aging phenomena and lifetime estimation of batteries in real cars.

This study demonstrates that electrochemical impedance spectroscopy (EIS) is useful for automotive purposes as EIS measurements are independent of pressure and orientation but sensitive to temperature and SOH. Thereby suggesting that work on an impedance-based BMS for automotive applications should continue.

Abbreviations and Formula Signs

BMS: Battery management system.
C: Battery capacity (i.e., charge content)
C_n: Nominal battery capacity (i.e., nominal charge content).
CCCV: Constant current constant voltage.
EIS: Electrochemical impedance spectroscopy.
I: Current.
OCV: Open circuit voltage.
PHEV: Plug-in hybrid electric vehicle.

RC: Resistance and capacitance.
SEI: Solid-electrolyte interface.
SNR: Signal-to-noise ratio.
SOC: State of charge.
SOH: State of health.

Acknowledgments

We would like to thank the Volkswagen AG for financial support.

Author Contributions

Simon Calles did the experimental work and data evaluation, Prof. Paul Heitjans gave professional advice and helped to improve the paper significantly and Dr. Alexander Börger organized the paper, made the conclusion and led the paper submission and review process.

Competing Interests

The authors have declared that no competing interests exist.

References

1. Hüttl RF, Pischetsrieder B, Spath D. Elektromobilität. Potenziale und wissenschaftlich-technische Herausforderungen. Heidelberg: Springer; 2010.
2. Yoshio M, Brodd RJ, Kozawa A. Lithium-ion batteries. New York: Springer; 2009.
3. Sarre G, Blanchard P, Broussely M. Aging of lithium-ion batteries. J Power Sources. 2004; 127: 65-71.
4. Zhang Q, White RE. Calendar life study of Li-ion pouch cells. J Power Sources. 2007; 173: 990-997.
5. Vetter J, Novák P, Wagner MR, Veit C, Möller KC, Besenhard JO, et al. Ageing mechanisms in lithium-ion batteries. J Power Sources. 2005; 147: 269-281.
6. Wohlfahrt-Mehrens M, Vogler C, Garche J. Aging mechanisms of lithium cathode materials. J Power Sources. 2004; 127: 58-64.
7. Arora P, White RE, Doyle M. Capacity fade mechanisms and side reactions in lithium-ion batteries. J Electrochem Soc. 1998; 145: 3647.
8. Broussely M, Biensan P, Bonhomme F, Blanchard P, Herreyre S, Nechev K, et al. Main aging mechanisms in Li ion batteries. J Power Sources. 2005; 146: 90-96.
9. Tröltzsch U, Kanoun O, Tränkler HR. Characterizing aging effects of lithium ion batteries by impedance spectroscopy. Electrochim Acta. 2006; 51: 1664-1672.
10. Burow D, Sergeeva K, Calles S, Schorb K, Börger A, Roth C, et al. Inhomogeneous degradation of graphite anodes in automotive lithium ion batteries under low-temperature pulse cycling conditions. J Power Sources. 2016; 307: 806-814.
11. Barsoukov E, Macdonald JR. Impedance spectroscopy. Theory, experiment, and applications. 2nd ed. Hoboken: John Wiley & Sons; 2005.
12. Orazem ME, Tribollet B. Electrochemical impedance spectroscopy. Hoboken: John Wiley & Sons; 2008.

13. Lvovich VF. Impedance spectroscopy: Applications to electrochemical and dielectric phenomena. Hoboken: John Wiley & Sons; 2012.
14. Meddings N, Heinrich M, Overney F, Lee J, Ruiz V, Napolitano E, et al. Application of electrochemical impedance spectroscopy to commercial Li-ion cells: A review. J Power Sources 2020; 480: 228742.
15. Gaberšček M. Understanding Li-based battery materials via electrochemical impedance spectroscopy. Nature Commun. 2021. 12: 6513.
16. Christophersen J, Morrison J, Morrison W, Motloch C. Rapid impedance spectrum measurements for state-of-health assessment of energy storage devices. SAE Int J Passeng Cars Electron Electr Syst. 2012; 5: 246-256.
17. Christophersen JP, Morrison JL, Motloch CG, Morrison WH. Long-term validation of rapid impedance spectrum measurements as a battery state-of-health assessment technique. SAE Int J Altern Powertrains. 2013; 2: 146-155.
18. Schmidt JP, Arnold S, Loges A, Werner D, Wetzel T, Ivers-Tiffée E. Measurement of the internal cell temperature via impedance: Evaluation and application of a new method. J Power Sources. 2013; 243: 110-117.
19. Srinivasan R, Carkhuff BG, Butler MH, Baisden AC. Instantaneous measurement of the internal temperature in lithium-ion rechargeable cells. Electrochim Acta. 2011; 56: 6198-6204.
20. Ecker M, Nieto N, Käbitz S, Schmalstieg J, Blanke H, Warnecke A, et al. Calendar and cycle life study of Li(NiMnCo)O_2-based 18650 lithium-ion batteries. J Power Sources. 2014; 248: 839-851.
21. Legrand N, Knosp B, Desprez P, Lapicque F, Raël S. Physical characterization of the charging process of a Li-ion battery and prediction of Li plating by electrochemical modelling. J Power Sources. 2014; 245: 208-216.
22. Karger A, Wildfeuer L, Maheshwari A, Wassiliadis N, Lienkamp M. Novel method for the on-line estimation of low-frequency impedance of lithium-ion batteries. J Energy Storage. 2020; 32: 101818.
23. Zhang C, Allafi W, Dinh Q, Ascencio P, Marco J. Online estimation of battery equivalent circuit model parameters and state of charge using decoupled least squares technique. Energy. 2018; 142: 678-688.
24. Dai H, Xu T, Zhu L, Wei X, Sun Z. Adaptive model parameter identification for large capacity Li-ion batteries on separated time scales. Appl Energy. 2016; 184: 119-131.
25. Hu Y, Wang YY. Two time-scaled battery model identification with application to battery state estimation. IEEE Trans Control Syst Technol. 2014; 23: 1180-1188.
26. Klotz D, Schönleber M, Schmidt JP, Ivers-Tiffée E. New approach for the calculation of impedance spectra out of time domain data. Electrochim Acta. 2011; 56: 8763-8769.
27. Maleki H, Howard JN. Internal short circuit in Li-ion cells. J Power Sources. 2009; 191: 568-574.

Enjoy *JEPT* by:

1. Submitting a manuscript
2. Joining in volunteer reviewer bank
3. Joining Editorial Board
4. Guest editing a special issue

For more details, please visit:
http://www.lidsen.com/journal/jept